

# A novel electrochemical DNA-sensing nanoplatform based on supramolecular ionic liquids grafted on nitrogen-doped graphene aerogels

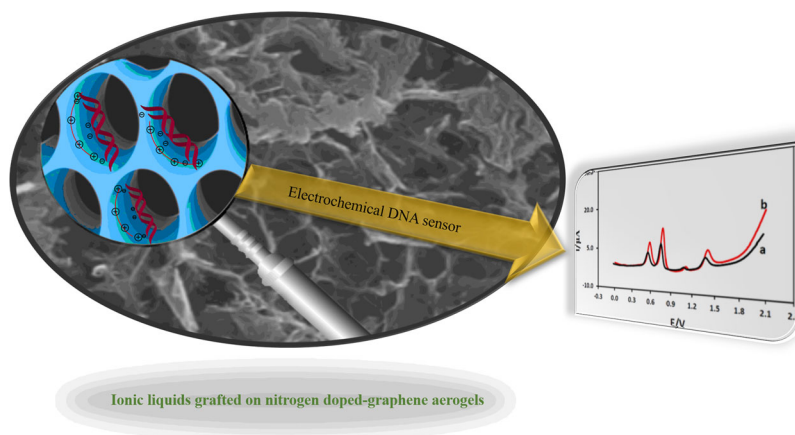
Hanif Kazerooni<sup>1</sup> · Bahram Nasernejad<sup>1</sup>

Received: 26 May 2015 / Accepted: 28 September 2015 / Published online: 5 November 2015  
© Springer Science+Business Media Dordrecht 2015

**Abstract** In this paper, the application of supramolecular ionic liquids grafted on nitrogen-doped graphene aerogels (SIL-g-(N)GAs), a novel electrode system, for the preparation of electrochemical DNA sensing platform is proposed. The super dispersion of SIL-g-(N)GAs in water makes it an ideal candidate for biological purposes such as gene delivery. In fact, SIL-g-(N)GAs/glassy carbon working electrode (GCE) can realize the simultaneous detection of all four DNA bases in double-stranded DNA without a prehydrolysis step. On the SIL-g-(N)GAs/GCE, due to the presence of SIL on the surface of three-dimensional nitrogen-doped graphene, the anchoring of the DNA probe

can be achieved by electrostatic association of SIL cations with the DNA backbone readily. So, herein we report a novel strategy for DNA hybridization without any electroactive tags or intercalators and suggest the potential applications of SIL-g-(N)GAs/GCE in the label-free electrochemical detection of DNA hybridization or DNA damage for further research. Moreover, the influence of potentially interfering substances on the determination of DNA is investigated.

## Graphical Abstract



**Electronic supplementary material** The online version of this article (doi:10.1007/s10800-015-0891-3) contains supplementary material, which is available to authorized users.

✉ Bahram Nasernejad  
banana@aut.ac.ir

<sup>1</sup> Faculty of Chemical Engineering, Amirkabir University of Technology (Tehran Polytechnic), 424 Hafez Ave, Tehran, 15875-4413, Iran

**Keywords** Biosensors · Electrochemical sensors · Nanotechnology · Nucleic acids · Polymers

## 1 Introduction

DNA detection methods have attracted considerable interest in the past few years due to their various applications including clinical diagnosis, environmental control, and forensic analysis [1–7]. Among the DNA detection methods, electrochemical-based methods are mostly used because these methods are very simple, rapid, and inexpensive compared with optical detections [3]. In 1960, Paleček reported one of the first electrochemical approaches to the detection of DNA involved the direct reduction of DNA at a dropping mercury electrode [8]. Thereafter, several concepts for DNA electroanalysis have been established including the direct DNA measurements, a hybridization-based technique with electroactive tags or intercalators, and an electron-transfer reaction through  $\pi$ -stacked DNA duplexes [1–3]. Among them, the direct DNA measurement is the simplest with various kinds of electrochemical methods. Mercury electrodes are suitable for studies involving DNA base reduction, while solid electrodes, such as carbon and metal electrodes, are used for oxidation processes. Despite allowing the high sensitivity of sensing based on the electrochemical reduction at a mercury electrode, the use of mercury is problematic which is due to the high affinity of DNAs for adsorption leading to non-specific DNA binding [9]. Thus, the development of DNA detection methods based on the direct oxidation of DNA has recently been studied more intensively [3]. Among the solid electrodes, carbon-based electrodes such as glassy carbon (GC) and boron-doped diamond (BDD) are widely used for direct detection of DNA because they have a wider potential window than metal electrodes and exhibit good electrochemical activity especially against aromatic compounds such as DNA bases. Although the conventional GC and BDD electrodes can detect guanine (G) and adenine (A), they cannot detect thymine (T) or cytosine (C). Some groups have recently reported that epitaxial graphene [10], chemically reduced graphene Oxide [11], anodized epitaxial graphene [12], graphene nanowalls [13], and electron cyclotron resonance (ECR) nanocarbon [14] electrodes may realize the simultaneous detection of all the four DNA bases (G, A, T, and C) in DNA.

Graphene, the two-dimensional  $sp^2$ -hybridized carbon, is a novel material that has emerged as a rapidly rising star in the field of electrochemistry due to its remarkable physicochemical properties [15]. One specific branch of graphene research deals with graphene oxide (GO) which

has great potential for providing new approaches and critical improvements in the field of electrochemistry [15, 16]. Graphene aerogels (GAs) represent a new class of ultralight and porous carbon materials that are associated with high strength-to-weight and surface-area-to-volume ratios [17–21]. More importantly, monolithic GAs consisting of 3D porous frameworks can provide multidimensional electron transport pathways [17–21]. The nitrogen doping of GAs is a new way in the field of electrochemistry which may prepare GAs-based electrodes with novel electrocatalytic properties and hold promise for design and prepare graphene-based electrodes for a wide range of applications in the field of electrochemistry. In addition, nitrogen doping is perhaps the most frequently chosen method, which can enhance the conductivity of graphene and graphene aerogels, and induces n-type semiconductor behavior [22, 23].

Modification of graphene with polymers (graphene nano-composites) has attracted extensive research interest [23–26]. Graphene nano-composite functionalized with poly ionic liquid has several advantages such as high dispersity, functionality, high specific surface area, and high surface charge density [27]. Therefore, this system can cause highly dispersive and long-term stable graphene sheets in reaction media [28–30]. Poly ionic liquid supported on particle surface due to liquid-like appearance called supramolecular ionic liquids (SILs) [31, 32]. In 2012, Senapati et al. demonstrated that ionic liquids are ideal media for long-term DNA storage through the electrostatic association of IL cations with the DNA backbone [33]. The SILs have higher surface charge density than ILs [27, 28], which this is a great feature for better interaction of SILs with DNA. Based on the told preface, the nitrogen doping of GAs and subsequent attachment of SILs to the surface of (N)-GAs is a novel strategy used to establish new electrochemical DNA systems with unique properties for direct oxidation of DNA. In this work, the supramolecular ionic liquids grafted on nitrogen-doped GAs (SIL-g-(N)GAs) were used as a new electrode system to direct detection of DNA.

## 2 Experimental

### 2.1 Materials and methods

All chemicals were purchased from Aldrich and used without further purification. IR spectra were recorded on a Bomem MB-Series FT-IR spectrophotometer. Transmission electron microscopy (TEM) analyzes were performed by LEO 912AB electron microscope. Ultrasonic bath (EUROSONIC® 4D ultrasound cleaner with a frequency of 50 kHz and an output power of 350 W) was used to

disperse materials in solvent. X-ray powder diffraction (XRD) data were collected on an XD-3A diffractometer using Cu K $\alpha$  radiation. Voltammetric experiments were performed using a  $\mu$ Autolab Type III electrochemical system. A conventional three-electrode cell consisting of a GCE (modified and unmodified), a platinum wire counter electrode, and a saturated Ag/AgCl reference electrode were used for voltammetric experiments. A digital pH-meter (Ion Analyzer 827, Metrohm) with precision of  $\pm 0.001$  was used for pH measurements. All electrochemical experiments were done at room temperature ( $25.0 \pm 1$  °C).

## 2.2 Preparation of the modified glassy carbon electrodes

Prior to the electrode modification process, a glassy carbon electrode (GCE) (2-mm diameter) was washed with deionized water and ethanol and then polishing was performed with 0.05  $\mu\text{m}$  alumina slurry on a polishing cloth. Typically, a stable suspension of SIL-g-(N)GAs/GCE containing 1.0 mg mL $^{-1}$  in DMF using 20 min ultrasonic agitation was prepared. The electrode surface was air dried, and 10.0  $\mu\text{L}$  of this suspension was cast onto the surface of the pretreated GC electrode with a microsyringe, and then it was dried in air. Furthermore, the suspension of (N)GAs/GCE and SIL-g-(N)GAs/GCE were prepared and used with the same procedure. The (N)GAs/GCE and SIL-g-(N)GAs/GCE show high dispersity and stability in DMF solution.

## 2.3 Plasma samples preparation

For analysis of plasma samples and recovery studies, a plasma sample (3.0 mL) was acidified with 100.0  $\mu\text{L}$  hydrochloric acid (37.0 %), and then, 150.0  $\mu\text{L}$  trichloroacetic acid (TCA) was added to denature the proteins. These processes eventually led to precipitation of proteins. Subsequently, the samples were centrifuged at 5000.0 rpm for 10.0 min. An amount of 2.0 mL of the supernatant was transferred to the voltammetric cell, and it was spiked with DNA at the desired concentration levels and then diluted 10.0 times with 0.1 M phosphate buffer at pH 3.0. The as-prepared solution was analyzed according to the procedure for voltammetric analysis.

## 2.4 Analytical procedure

After fabricating each electrode, to obtain reproducible current–potential curves, cyclic voltammetry (CV) was performed at scan rate of 100.0 mV s $^{-1}$  between  $-0.8$  and 1.0 V for 10.0 times in 0.1 M in phosphate buffer solution. In addition, the buffer solution was purged with high-purity nitrogen for at least 10.0 min prior to each electrochemical

measurement. The impedance measurements were performed with an Autolab (PG stat 302 N) in 0.1 M KCl solution containing 0.5 mM Fe(CN) $_6^{3-}/4-$  in the frequency range from 0.1 Hz to 100 kHz. A sinusoidal potential modulation of  $\pm 0.01$  V amplitude was superimposed on the formal potential of the redox couple of [Fe(CN) $_6^{4-}$ ]/[Fe(CN) $_6^{3-}$ ] (0.22 V versus Ag/AgCl). Prior to the experiments, the electrolyte solutions were deoxygenated by bubbling with high-purity nitrogen for at least 20 min. All experiments were carried out at room temperature.

## 3 Materials preparation

### 3.1 Synthesis of SIL-g-(N)GAs

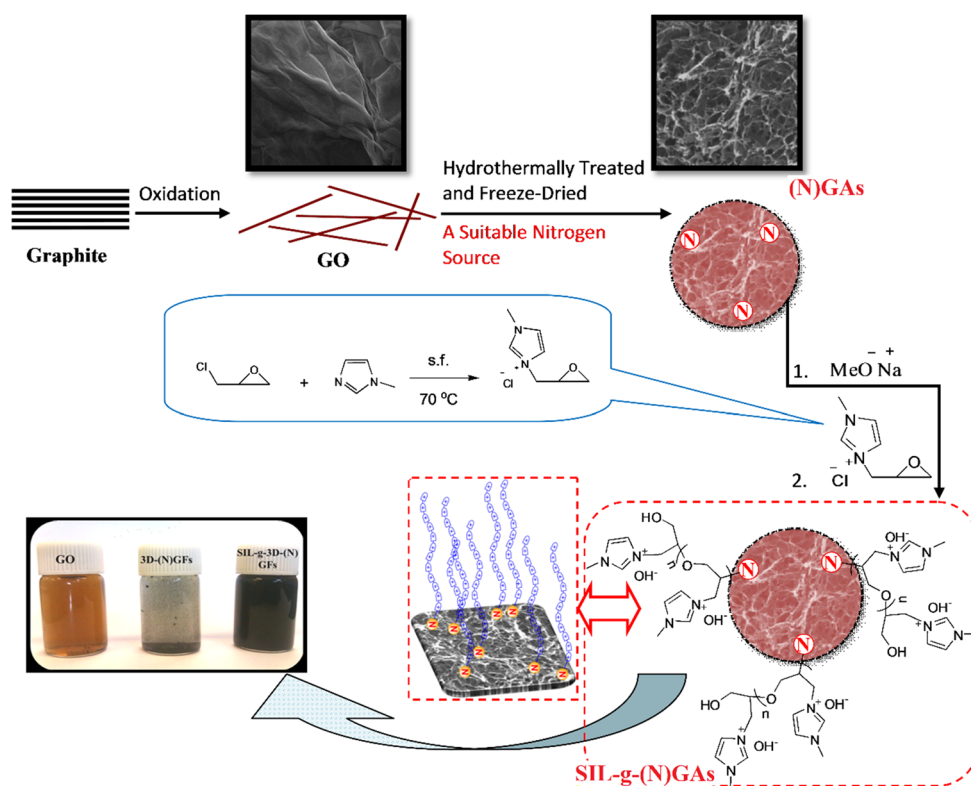
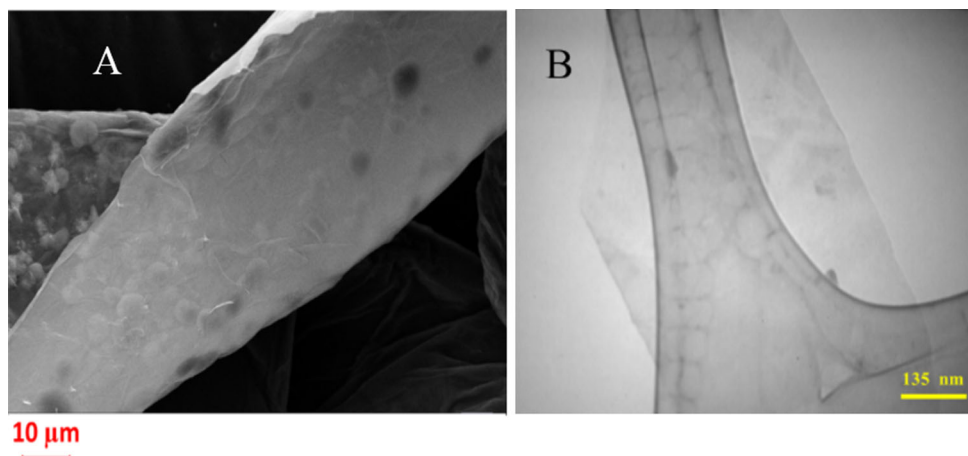
The SIL-g-(N)GAs were synthesized according to our previous report [34]. Briefly, graphene oxide (GO) was synthesized by Hummer method [35]. Then, (N)GAs were synthesized with a combined hydrothermal and freeze-drying process [21, 36]. (N)GAs (0.5 g) and cesium hydroxide monohydrate (3.0 g) were placed in a 250-mL Schlenk flask, and 20 mL toluene was added. The mixture was stirred at 60 °C under an argon atmosphere for 1 h to generate the corresponding cesium alkoxide and evacuated at 60 °C for 12 h to remove the toluene and water. Subsequently, 20 mL dry THF was transferred into the Schlenk flask. 1-methyl-3-(oxiran-2-ylmethyl)-1H-imidazol-3-ium chloride was transferred to a graduated ampoule and then transferred into the reaction flask containing the above mixture. The mixture was heated at 60 °C and stirred for at least 12–24 h. The polymer solution was dried under vacuum and dialyzed against deionized water. Finally, a highly viscous black liquid-like product was obtained. Solid potassium hydroxide was used to replace the chloride ion on the SIL-g-(N)GAs with a hydroxide ion by adding both to water (50 mL) and stirring vigorously at room temperature for 24 h. Then, the mixture was centrifuged, washed with water, and dried under reduced pressure to give the supported basic SIL-g-(N)GAs [34].

## 4 Results and discussion

### 4.1 Synthesis and characterization of SIL-g-(N)GAs

The synthesis of supramolecular ionic liquids grafted on nitrogen-doped graphene aerogels as the chosen support material was accomplished according to our recently report as shown schematically in Scheme 1.

Typical scanning electron microscopy (SEM) image of the suspended GO sheets has been shown in Fig. 1. SEM is used to obtain information about the morphologies and

**Scheme 1** Synthesis of SIL-g-(N)GAs**Fig. 1** SEM (a) and TEM (b) images of GO

sample surfaces. The exfoliated graphene sheets with lateral dimensions of several micrometers were observed in SEM images. Figure 1b shows TEM image of GO, drop casted onto a lacey carbon grid, that it clearly deduced the few layers and very high quality of GO.

The 3D morphology and size of the as-prepared (N)GAs were confirmed by SEM images. Figure 2a, b shows an interconnected framework of ultrathin graphene nanosheets with porous structure. As can be seen, the pore size is ranging from a few hundred nanometers to several micrometers. The surface area in porous materials is an important factor affecting the loading of SILs. So,

Brunauer-Emmett-Teller (BET) method was used to estimate the surface area of the as-prepared (N)GAs.

Nitrogen adsorption–desorption analysis reveals a typical BET surface area of up to  $266.0 \text{ m}^2 \text{ g}^{-1}$  for (N)GAs.  $\text{N}_2$  adsorption–desorption isotherm of (N)GAs has been given in Fig. 3. Therefore, the synthesized support has high surface area to embed SILs and subsequently nucleic acid. The chemical composition of GO, (N)GAs, and SIL-g-(N)GAs was confirmed by FT-IR, X-ray powder diffraction (XRD), and X-ray photoelectron spectroscopy (XPS) (See ESI).

The electron-transfer capabilities of the GO-, (N)GA-, and SIL-g-(N)GA-modified electrodes were investigated

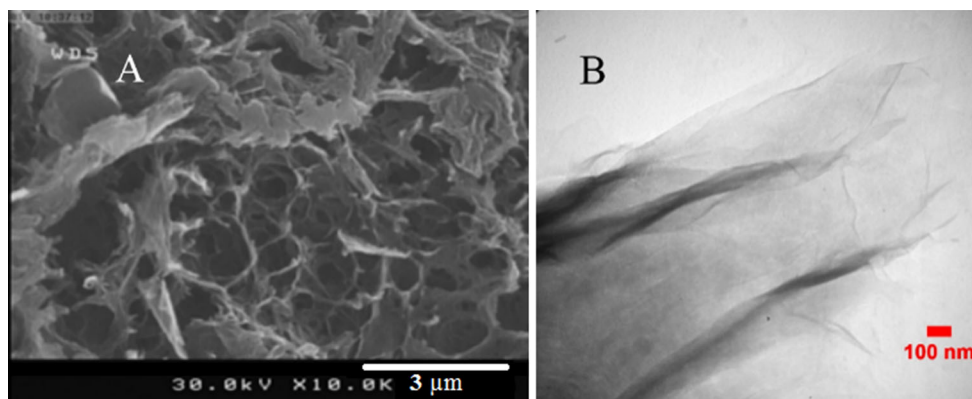


**Fig. 2** SEM (a) and TEM (b) images of (N)GAs

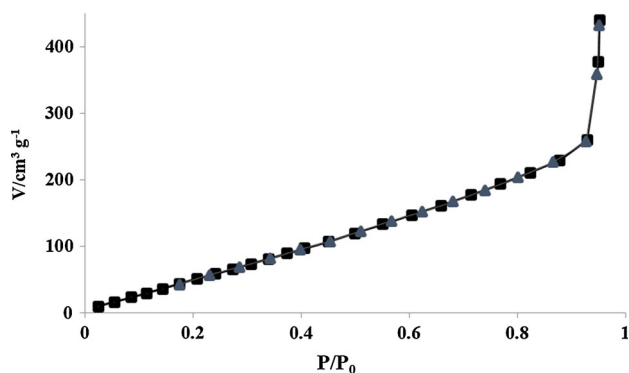


**Fig. 3**  $N_2$  adsorption–desorption isotherm of (N)GAs

by electrochemical impedance spectroscopy (Fig. 4). In all samples, electrolyte resistance ( $R_s$ ) is approximately  $5 \Omega$  showing the similar medium condition and the low electrolyte resistance. In higher frequencies, the electrical double layer ( $C_{dl}$ ) was observed as a semicircle. In the middle frequencies, the semicircle changed to a horizontal line demonstrating the charge transfer resistance ( $R_{ct}$ ). As observed, the charge transfer resistances were reduced with enhancing the sample function. The charge transfer in the GO-modified electrode was  $154 \Omega$  while the charge transfer of the (N)GA- and SIL-g-(N)GA-modified electrodes were decreased to  $69.2$  and  $26.4 \Omega$ . The scope of the mass transfer region is approximately similar in all samples, which demonstrates the same mass transfer resistance.

#### 4.2 Direct DNA detection

Before employing the sensor for electrooxidation and analytical measurements of Cysteine (CySH), the electrochemical properties of the electrodes were studied by cyclic voltammetry. The CVs of the GCE, GO/GCE, (N)GAs/GCE, SIL-g-(N)GAs/GCE are shown in Fig. 5. The SIL-g-(N)GAs/GCE has a maximum background current, which can be related to the positive surface charge

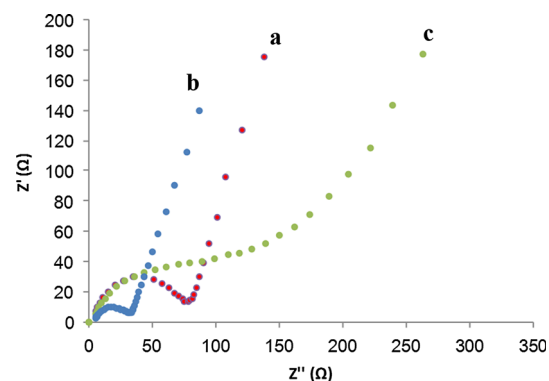


**Fig. 4** Nyquist plots of GO- (a), (N)GA- (b), and SIL-g-(N)GA- (c) modified electrodes in  $0.1 \text{ M KCl}$  solution containing  $0.5 \text{ mM Fe(CN)}_6^{3-/4-}$

of the SIL. To further confirm the positive charge of SIL from the electrochemistry viewpoint, the electrochemical behaviors of SIL-g-(N)GAs/GCE, (N)GAs/GCE, and GO/GCE in the presence of  $\text{Fe(CN)}_6^{3-/4-}$  were studied (Fig. 6). As seen in Fig. 6, between three electrode systems,  $\text{Fe(CN)}_6^{3-/4-}$  has a higher redox current peak on the surface of SIL-g-(N)GAs/GCE, which is due to the attraction forces between positive and negative charge centers.  $\text{Fe(CN)}_6^{3-/4-}$  (negatively charged) has the highest tendency to attract on the surface of SIL-g-(N)GAs/GCE (positively charged) compared to (N)GAs/GCE and GO/GCE, and this attraction can increase the redox current peaks.

To study the potential application of new sensor, the direct sensing of DNA by monitoring the oxidation current of its nucleic acids was investigated using differential pulse voltammetry (DPV). The differential pulse voltammetric (DPV) signals for the oxidation of all DNA bases at the GO/GCE (a), GAs/GCE (b), (N)GAs/GCE (c), and SIL-g-(N)GAs/GCE (d) are shown in Fig. 7.

The oxidation of dsDNA on the surface of GO/GCE (a), GAs/GCE (b), (N)GAs/GCE (c), and SIL-g-(N)GAs/GCE gives four well-anodic peaks with high resolutions for G,



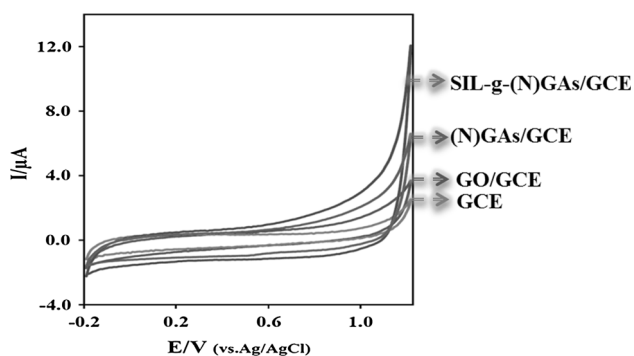


**Fig. 5** CVs for GCE, GO/GCE, (N)GAs/GCE, and SIL-g-(N)GAs/GCE in 0.1 M pH 7 phosphate buffer solution. Scan rate  $50 \text{ mV s}^{-1}$

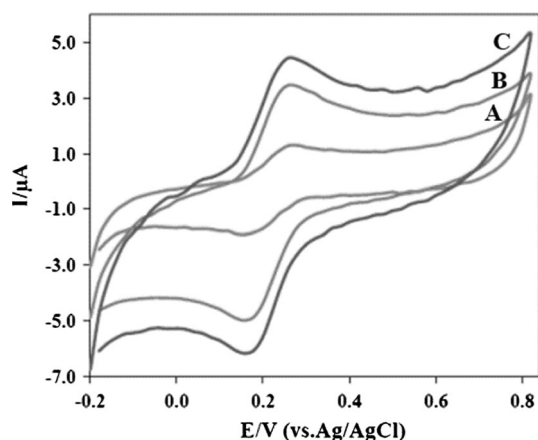


**Fig. 6** CVs for 0.1 mM  $\text{Fe}(\text{CN})_6^{3-/4-}$  in 1 M KCl at GO/GCE (a), (N)GAs (b), SIL-g-(N)GAs/GCE (c). Scan rate  $50 \text{ mV s}^{-1}$

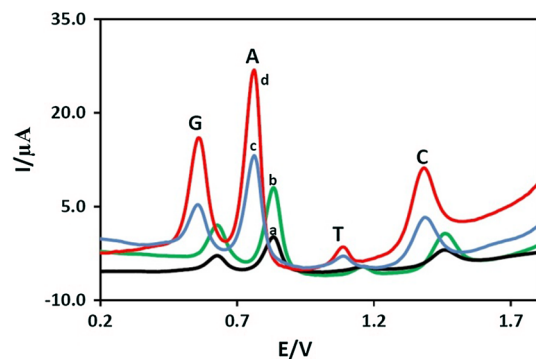


**Fig. 7** DPVs for free DNA bases ( $50 \mu\text{M}$  equimolar mixture of G, A, T, and C) at GO/GCE (a), GAs/GCE (b), (N)GAs/GCE (c), and SIL-g-(N)GAs/GCE (d). Electrolyte 0.1 M pH 7.0 phosphate buffer solution

A, T, and C, which their peak potentials and peak currents are different. As compared with GCE, GAs exhibited larger peak currents for the oxidation of DNA bases, which is related to the high specific surface areas of GAs. Furthermore, as compared with GO and GAs, (N)-GAs/GCE

exhibited larger peak currents and more negative peak potentials for the oxidation of dsDNA.

The results suggested that nitrogen doping in GAs has a synergistic effect on the oxidation of dsDNA. Moreover, the oxidation reaction of dsDNA is facilitated in (N)-GAs/GCE than GO and GAs. Additionally, in the surface of (N)-GAs/GCE, the oxidation potentials for G, A, and C are lower than those obtained from chemically reduced graphene oxide-modified glassy carbon electrode [10], anodized epitaxial graphene (EG) electrode [11], and graphene nanowalls [12], and that for T are near to that. When the electrode was modified with SIL-g-(N)GAs, as compared to others electrode, the maximum peak current was obtained for DNA bases. This proves the success of DNA immobilization and also indicates a higher density of DNA coverage. The DNA immobilization on SIL-g-(N)GAs/GCE can be justified by electrostatic interaction between positive charge on SILs and negative charge on DNA (negative charges of phosphate groups).

In this case, the maximum peak current and lower oxidation peaks on the (N)GAs/GCE can be convinced to result from the combination of two factors: one is the catalytic activity of the (N)GAs and the other one is the positive charge on SILs which it can facilitate or mediate the charge/electron transfer between DNA bases and the electrode surface, and modulate the electrochemical reactions in a controlled fashion. Based on above explanation, both nitrogen doping and GAs clearly play an important role and have synergistic effect in the oxidation of all the free DNA bases.

In addition, the remarkable performance of this method is the ability of SIL-g-(N)GAs/GCE to simultaneously detect of all four DNA bases without a prehydrolysis step which is the unique advantage. Previous studies showed that except from a few methods [3], other procedures for the detection of DNA bases need a prehydrolysis step to release the bases into their free states. Moreover, the studies indicated that with increasing the number of DPV up to 50 cycles, the SIL-g-(N)GAs/GCE electrode exhibited a stable response to DNA bases with a slight decrease (about 7 %) in the intensity of the peak currents. These results demonstrated that the simultaneous detection of DNA bases at the SIL-g-(N)GAs/GCE would result from the antifouling properties and the fast electron-transfer kinetics for bases oxidation at the SIL-g-(N)GAs.

To evaluate the capability of the SIL-g-(N)GAs/GCE, the technique was tested for detection of different concentrations of DNA (Fig. 8). As can be seen, the height of the DPV peaks for the oxidation of all DNA bases ( $I_{pa}$ ) linearly increases with increasing DNA concentrations. There are linear relationships between the DPV oxidation current values ( $I_p$ ) based on G, A, T, and C with the DNA

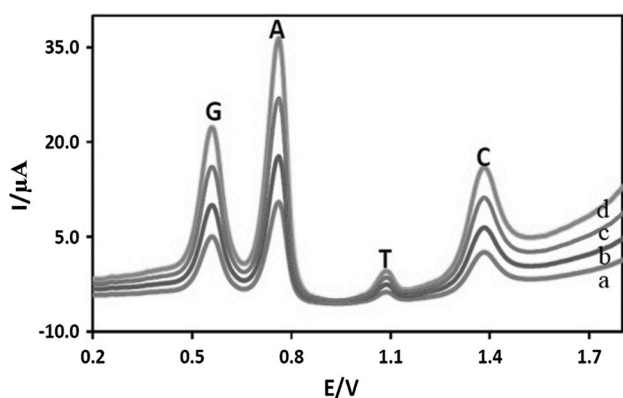


**Fig. 8** DPVs at the SIL-g-(N)GAs/GCE at different dsDNA concentrations (a → d): 0.01, 30, 60, and 100 nM

concentrations (C) in the range of 5 pM–200 nM (Fig. 8). The regression equations were as follows:

For G:  $I_p (\mu A) = 0.203 G (nM) + 7.542 (R^2 = 0.996)$ .  
 For A:  $I_p (\mu A) = 0.343 A (nM) + 14.66 (R^2 = 0.998)$ .  
 For T:  $I_p (\mu A) = 0.077 T (nM) + 0.649 (R^2 = 0.998)$ .  
 For C:  $I_p = 0.132 C (nM) + 4.637 (R^2 = 0.997)$ .

A limit of detection (LOD) of 2 pM was obtained. In order to evaluate a voltammetric method, with respect to

the low LOD (2 pM), the proposed method was applied to determine DNA in plasma samples. The recovery studies were carried out by spiking-free plasma with known amounts of DNA (standard addition method), and the calibration plot was used for determination of spiked DNA in human plasma. The results for detection of DNA in three samples are presented in Table 1. The recoveries were determined in the range of 96.7–105.0 % with RSD (%) below 3.0 %. The results illustrated that the proposed method is accurate enough for practical applications.

For further studies, Under the same experimental conditions, the potential application of SIL-g-(N)GAs/GCE for simultaneous detection of all the free DNA bases was evaluated (Fig. 9). The SIL-g-(N)GAs/GCE shows remarkable response to the concentration changes of each free DNA base (Fig. 9), and the anodic peak currents for each free DNA base increased with increasing their concentrations. Therefore, each free DNA base is effectively detected by oxidation on the SIL-g-(N)GAs/GCE.

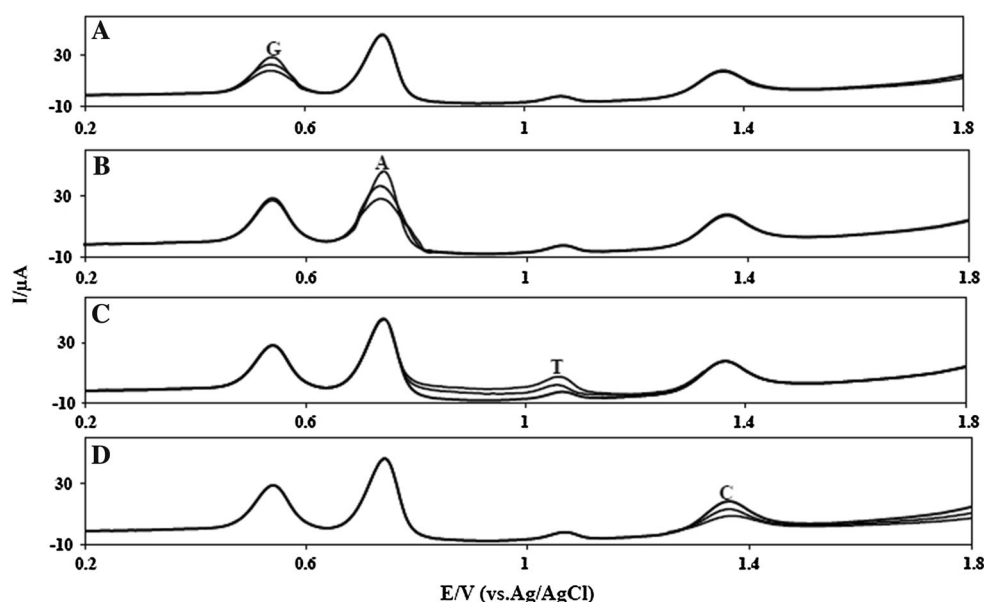
In addition, the potential application of SIL-g-(N)GAs/GCE for different DNA sequences was tested using wild-type oligonucleotide 5'-CATGAAC TG-3' and 5'-GCTA CCCTTGC-3' (Scheme 2).

**Table 1** Determination of DNA in plasma samples

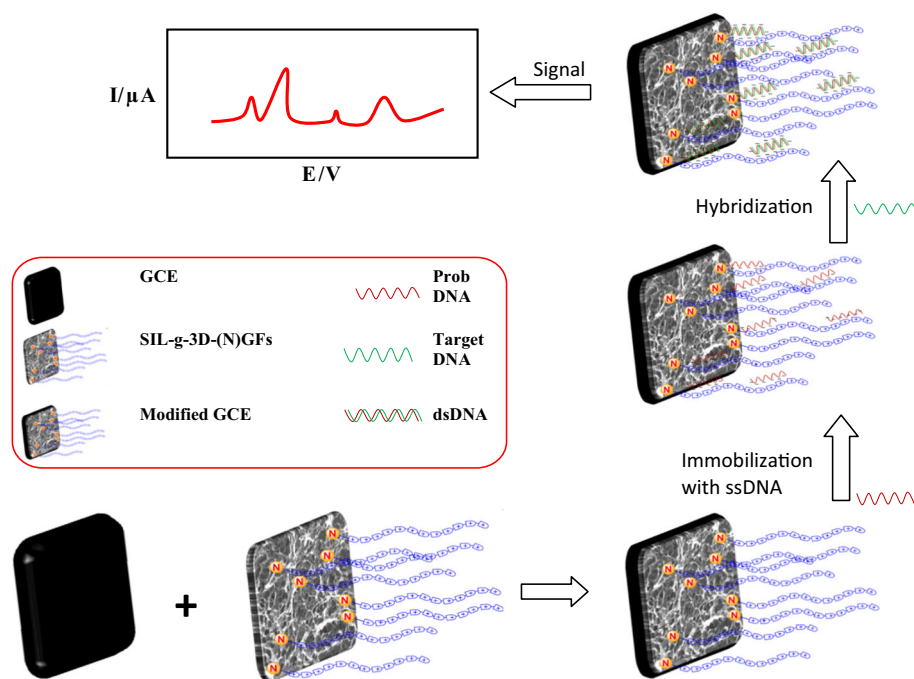
Plasma	Spiked (nM)	Found ( $10^{-6}$ M) <sup>a</sup>	Recovery (%) + RSD %
Sample 1	1	1.04	105 ± 1.6
Sample 2	3	2.9	96.7 ± 1.85
Sample 3	7	7.1	101.4 ± 1.7

<sup>a</sup> Average of six determinations

**Fig. 9** DPVs for free DNA bases **a** 10, 25, and 50 μM of G in the presence of 50 μM equimolar mixture of A, T, and C, **b** 10, 25, and 50 μM of A in the presence of 50 μM equimolar mixture of G, T, and C, **c** 50, 75, and 100 μM of T in the presence of 50 μM equimolar mixture of G, A, and C, and **d** 10, 25, and 50 μM of C in the presence of 50 μM equimolar mixture of G, A, and T



**Scheme 2** Potential application of SIL-g-(N)GAs/GCE for different DNA sequences



As can be observed from Fig. 10, the difference between DNA sequences clearly marked from the difference between the DPVs of 1 and 2 at the SIL-g-(N)GAs/GCE (Fig. 10). These results presented the applicability of technique to detect a DNA sequence for short oligomers with a particular sequence at physiological pH without any hybridization or labeling processes. These results could be associated to the ability of SIL-g-(N)GAs/GCE to quantitatively measure the total content of each base in the oligonucleotides, which is comparable with that of ECR nanocarbon film electrode [13] and chemically reduced graphene oxide [10].

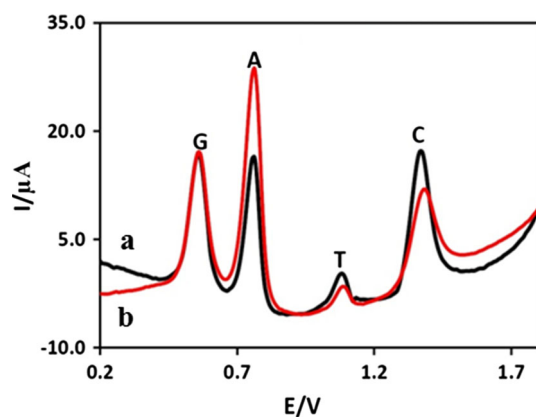


**Fig. 10** Detection of DNA including the different sequences 5'-GCT ACCCTGC-3' (a) and 5'-CATGAACTG-3' (b) (0.1 μM DNA). Electrolyte 0.1 M pH 7.0 phosphate buffer solution

### 4.3 DNA hybridization

To examine the ability of the method to enhance the signal-to-noise ratio in bioaffinity events, the biofunctionalization of SIL-g-(N)GAs/GCE with DNA was investigated. For immobilization of the probe DNA (p-ssDNA, 5'-TTGAC ACCAGACCAACTGGT-3') onto the SIL-g-(N)GAs/GCE, after electrode pretreatment, it was kept in the immobilization solution containing 1 nM p-ssDNA for 3 min (optimum time). At the end of the grafting, the electrode was rinsed thoroughly with the immobilization buffer, and then its DPV was recorded in a 0.1 M phosphate solution without p-ssDNA (Fig. 11a). As shown in Fig. 11a, after DNA immobilization, well-defined oxidation peaks for DNA bases were observed. It proves the success immobilization of DNA and also indicates a higher density of DNA coverage. The DNA immobilization on SIL-g-(N)GAs/GCE can be justified by electrostatic interaction between positive charge on SILs and negative charge on p-ssDNA (negative charges of phosphate groups).

The performance of the immobilized p-ssDNA chains on the SIL-g-(N)GAs/GCE for sequence-specific DNA diagnoses is demonstrated in Fig. 11. In this step, the immobilized p-ssDNA/SIL-g-(N)GAs/GCE was placed for 5 min in a solution containing 5 nM complementary ssDNA (c-ssDNA, 5'-ACCAGTTGGTCTGGTGTCAA-3') for hybridizing with the surface-immobilized p-ssDNA to form double-strand DNA (dsDNA) helices on the SIL-g-(N)GAs/GCE. Then the electrode was rinsed thoroughly with the immobilization buffer, and then in a 0.1 M phosphate solution, without



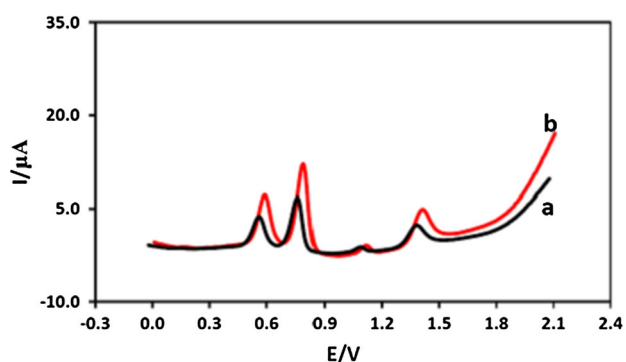


**Fig. 11** The DPV curve of ssDNA after DNA immobilization in 1 nM ssDNA for 3 min (a) and The DPV curve of dsDNA after hybridization step (b). Electrolyte 0.1 M pH 7.0 phosphate buffer solution

c-ssDNA and p-ssDNA, its DPV was recorded (Fig. 11b). The results showed the increase in the oxidation peak due to the hybridization. Upon hybridization with the c-ssDNA, more DNA bases are susceptible to oxidation reactions which cause an increase in the oxidation current peaks. These results indicated the ability of an immobilized p-ssDNA/SIL-g-(N)GAs/GCE to recognize and hybridize with a complementary ssDNA in the recognition interface. To confirm this claim, the addition of non-complementary DNA chains (5'-CTCCAGGAGTCGTCGCCACC-3') in the hybridization step under the same conditions did not show any significant changes in DNA bases' oxidation peaks. This indicates that, as expected, there was no specific DNA pairing interaction with the non-complementary DNA chains.

The reproducibility of the proposed method was studied by detecting 1 nM target DNA using five independent electrodes. The relative standard deviation was found to be 6.2 %, indicating satisfactory reproducibility.

Some inorganic ions and organic compounds may coexist with DNA in biological samples (such as plasma), and these compounds can affect the voltammetric response of the DNA. Thus, in order to evaluate the specificity of the proposed method, the influence of potentially interfering substances such as  $Mg^{2+}$ ,  $Ca^{2+}$ ,  $Cu^{2+}$ ,  $Zn^{2+}$ ,  $Fe^{3+}$ ,  $Na^+$ ,  $K^+$ ,  $SO_4^{2-}$ ,  $Cl^-$ , nitrate, glucose, fructose, sucrose, talc, citric acid, dopamine, ascorbic acid (AA), and uric acid (UA) on the determination of DNA was investigated by using DPV. The results indicated that no interference was observed on the signals of DNA in the presence of interfering substances with concentration of 1000.0-fold to DNA with a deviation below 5.0 %. It was observed that the method can be safely applied for determination of DNA in biological samples.

Most of the hybridization biosensors are the label-based methods which concentrated on using redox indicators to differentiate between single and double strands of DNA on

the electrode. The main advantage of this method is being label free which is simple and sensitive and also eliminating the need to complex procedures for measuring hybridization process and removing the need to redox indicators to identify the hybridization step.

## 5 Conclusions

We have developed an electrochemical DNA detection method based on supramolecular ionic liquids grafted on nitrogen-doped graphene aerogel-modified glassy carbon electrode. This method is able to DNA detection, DNA hybridization, and DNA sequencing. Furthermore, this DNA biosensor, with no need of any kind of enzyme, label, or sophisticated equipment, is really simple and inexpensive.

## References

1. Drummond TG, Hill MG, Barton JK (2003) Electrochemical DNA sensors. *Nat Biotechnol* 21(10):1192–1199
2. Park S-J, Taton TA, Mirkin CA (2002) Array-based electrical detection of DNA with nanoparticle probes. *Science* 295(5559):1503–1506
3. Paleček E, Bartošík M (2012) Electrochemistry of nucleic acids. *Chem Rev* 112(6):3427–3481
4. Song S, Qin Y, He Y, Huang Q, Fan C, Chen H-Y (2010) Functional nanoprobe for ultrasensitive detection of biomolecules. *Chem Soc Rev* 39(11):4234–4243
5. Li D, Song S, Fan C (2010) Target-responsive structural switching for nucleic acid-based sensors. *Acc Chem Res* 43(5):631–641
6. Dong H, Gao W, Yan F, Ji H, Ju H (2010) Fluorescence resonance energy transfer between quantum dots and graphene oxide for sensing biomolecules. *Anal Chem* 82(13):5511–5517
7. Guo Y, Deng L, Li J, Guo S, Wang E, Dong S (2011) Hemigraphene hybrid nanosheets with intrinsic peroxidase-like activity for label-free colorimetric detection of single-nucleotide polymorphism. *ACS Nano* 5(2):1282–1290
8. Paleček E (1960) Oscillographic polarography of highly polymerized deoxyribonucleic acid. *Nature* 188:656–657
9. Batchelor-McAuley C, Wildgoose GG, Compton RG (2009) The physicochemical aspects of DNA sensing using electrochemical methods. *Biosens Bioelectron* 24(11):3183–3190
10. Lim CX, Hoh HY, Ang PK, Loh KP (2010) Direct voltammetric detection of DNA and pH sensing on epitaxial graphene: an insight into the role of oxygenated defects. *Anal Chem* 82(17):7387–7393
11. Zhou M, Zhai Y, Dong S (2009) Electrochemical sensing and biosensing platform based on chemically reduced graphene oxide. *Anal Chem* 81(14):5603–5613
12. Dubuisson E, Yang Z, Loh KP (2011) Optimizing label-free DNA electrical detection on graphene platform. *Anal Chem* 83(7):2452–2460
13. Akhavan O, Ghaderi E, Rahighi R (2012) Toward single-DNA electrochemical biosensing by graphene nanowalls. *ACS Nano* 6(4):2904–2916

14. Kato D, Sekioka N, Ueda A, Kurita R, Hirono S, Suzuki K, Niwa O (2008) Nanohybrid carbon film for electrochemical detection of SNPs without hybridization or labeling. *Angew Chem Int Ed* 47(35):6681–6684
15. Chen D, Feng H, Li J (2012) Graphene oxide: preparation, functionalization, and electrochemical applications. *Chem Rev* 112(11):6027–6053
16. Georgakilas V, Otyepka M, Bourlinos AB, Chandra V, Kim N, Kemp KC, Hobza P, Zboril R, Kim KS (2012) Functionalization of graphene: covalent and non-covalent approaches, derivatives and applications. *Chem Rev* 112(11):6156–6214
17. Wu Z-S, Sun Y, Tan Y-Z, Yang S, Feng X, Müllen K (2012) Three-dimensional graphene-based macro- and mesoporous frameworks for high-performance electrochemical capacitive energy storage. *J Am Chem Soc* 134(48):19532–19535
18. Worsley MA, Pauzauskie PJ, Olson TY, Biener J, Satcher JH, Baumann TF (2010) Synthesis of graphene aerogel with high electrical conductivity. *J Am Chem Soc* 132(40):14067–14069
19. Xu Y, Wu Q, Sun Y, Bai H, Shi G (2010) Three-dimensional self-assembly of graphene oxide and DNA into multifunctional hydrogels. *ACS Nano* 4(12):7358–7362
20. Chen Z, Ren W, Gao L, Liu B, Pei S, Cheng H-M (2011) Three-dimensional flexible and conductive interconnected graphene networks grown by chemical vapour deposition. *Nat Mater* 10(6):424–428
21. Wu ZS, Winter A, Chen L, Sun Y, Turchanin A, Feng X, Müllen K (2012) Three-dimensional nitrogen and boron co-doped graphene for high-performance all-solid-state supercapacitors. *Adv Mater* 24(37):5130–5135
22. Wei D, Liu Y, Wang Y et al (2009) Synthesis of N-doped graphene by chemical vapor deposition and its electrical properties. *Nano Lett* 9:1752–1758
23. Wang X, Li X, Zhang L et al (2009) N-doping of graphene through electrothermal reactions with ammonia. *Science* 324:768–771
24. Lotya M, King PJ, Khan U, De S, Coleman JN (2010) High-concentration, surfactant-stabilized graphene dispersions. *ACS Nano* 4(6):3155–3162
25. Patil AJ, Vickery JL, Scott TB, Mann S (2009) Aqueous stabilization and self-assembly of graphene sheets into layered bio-nanocomposites using DNA. *Adv Mater* 21(31):3159–3164
26. Shih C-J, Lin S, Strano MS, Blankschtein D (2010) Understanding the stabilization of liquid-phase-exfoliated graphene in polar solvents: molecular dynamics simulations and kinetic theory of colloid aggregation. *J Am Chem Soc* 132(41):14638–14648
27. Lonkar SP, Bobenrieth A, De Winter J, Gerbaux P, Raquez J-M, Dubois P (2012) A supramolecular approach toward organo-dispersible graphene and its straightforward polymer nanocomposites. *J Mater Chem* 22(35):18124–18126
28. Ji Q, Honma I, Paek S-M, Akada M, Hill JP, Vinu A, Ariga K (2010) Layer-by-layer films of graphene and ionic liquids for highly selective gas sensing. *Angew Chem Int Ed* 49(50):9737–9739
29. Ul Hasan K, Sandberg MO, Nur O, Willander M (2011) Polycation stabilization of graphene suspensions. *Nano Res Lett* 6(1):1–6
30. Zhou X, Wu T, Ding K, Hu B, Hou M, Han B (2010) Dispersion of graphene sheets in ionic liquid [bmim][PF6] stabilized by an ionic liquid polymer. *Chem Commun* 46(3):386–388
31. Texter J, Qiu Z, Crombez R, Byrom J, Shen W (2011) Nanofluid acrylate composite resins-initial preparation and characterization. *Polym Chem* 2(8):1778–1788
32. Zeng C, Tang Z, Guo B, Zhang L (2012) Supramolecular ionic liquid based on graphene oxide. *Phys Chem Chem Phys* 14(28):9838–9845
33. Chandran A, Ghoshdastidar D, Senapati S (2012) Groove binding mechanism of ionic liquids: a key factor in long-term stability of DNA in hydrated ionic liquids? *J Am Chem Soc* 134(50):20330–20339
34. Kazerooni H, Nassernejad B (2014) Synthesis of supramolecular ionic liquid grafted three-dimensional nitrogen-doped graphene as a modified cationic polymer. *RSC Adv* 4:34604–34609
35. Hummers WS, Offeman RE (1958) Preparation of graphitic oxide. *J Am Chem Soc* 80(6):1339
36. Zhao Y, Hu C, Hu Y, Cheng H, Shi G, Qu L (2012) A versatile, ultralight, nitrogen-doped graphene framework. *Angew Chem Int Ed* 124(45):11174–11177